

General method of solid angle calculation using attitude kinematics

Russell P. Patera¹

351 Meredith Way, Titusville, FL 32780, United States

Abstract

A general method to compute solid angle is developed that is based on Ishlinskii's theorem, which specifies the relationship between the attitude transformation of an axis that completely slews about a conical region and the solid angle of the enclosed region. After an axis slews about a conical region and returns to its initial orientation, it will have rotated by an angle precisely equal to the enclosed solid angle. The rotation is the magnitude of the Euler rotation vector of the attitude transformation produced by the slewing motion. Therefore, the solid angle can be computed by first computing the attitude transformation of an axis that slews about the solid angle region and then computing the solid angle from the attitude transformation. This general method to compute the solid angle involves approximating the solid angle region's perimeter as seen from the source, with a discrete set of points on the unit sphere, which join a set of great circle arcs that approximate the perimeter of the region. Pivot Parameter methodology uses the defining set of points to compute the attitude transformation of the axis due to its slewing motion about the enclosed solid angle region. The solid angle is the magnitude of the resulting Euler rotation vector representing the transformation. The method was demonstrated by comparing results to published results involving the solid angles of a circular disk radiation detector with respect to point, line and disk shaped radiation sources. The proposed general method can be applied to any detector-source geometric configuration.

Keywords: solid angle, geometrical efficiency, Ishlinskii's theorem, Attitude kinematics, radiation source-detector geometry

Nomenclature

A	semi-major axis of ellipse
a(k)	x-component
B	semi-minor axis of ellipse
b(k)	y-component
dL	increment of line source
d	shift distance of parallel disk axis
G(k)	solid angle of disk detector at kth point
GE	geometrical efficiency
G1	solid angle of 1 st Gaussian integration point
G2	solid angle of 2 nd Gaussian integration point
h	height of source above detector plane
I	integration of solid angle over region
I _E	integration of solid angle over enlarged region
I _S	integration of solid angle over source disk
L1	beginning of line source
L2	end of line source
R	radius of detector

¹ Russell.p.patera@gmail.com

1	R_0	radius of expanded detector
2	$\mathbf{R}(r, \alpha)$	rotational transformation about r by α
3	$\mathbf{r}(m)$	midpoint of line segment
4	\mathbf{S}_1	1 st point of Gaussian integration
5	\mathbf{S}_2	2 nd pint of Gaussian integration
6	$\mathbf{S}(k)$	k th point of line source
7	\mathbf{S}	source location
8	\sin_1	sine of 1 st Gaussian angle
9	\sin_2	sine of 2 nd Gaussian angle
10	$\mathbf{U}(a, b)$	slewing transformation from a to b
11	\mathbf{V}	Euler rotation vector
12	$x(m)$	x coordinate of midpoint of line segment
13	$y(m)$	y coordinate of midpoint of line segment
14	Ω	solid angle
15	Ω_S	solid angle of detector seen from source
16	Ω_R	solid angle of source seen from detector
17	Φ	polar angle
18	Φ_1	1 st Gaussian integration angle
19	Φ_2	2 nd Gaussian integration angle
20	ρ	radius of disk source
21	$\Psi(\mathbf{a})$	$\mathbf{R}(\mathbf{a}, 180)$
22	Θ	polar angle
23	Θ_1	1 st Gaussian integration angle
24	Θ_2	2 nd Gaussian integration angle

25

26 1. Introduction

27 The need to evaluate the solid angle appears in very diverse areas ranging from radiant heat transfer, particle
 28 scattering cross sections, electric and magnetic field strength around charge distributions, evaluating the size of
 29 ligands in metal complexes, and calibrating the strength of radioisotopes by computing the geometrical efficiency
 30 of various source and detector geometries. The methods used to compute solid angle start with the fundamental
 31 integral equation and employ various mathematical methods to compute the integral. Paxton (1959), found a
 32 general expression for the solid angle subtended by a circular disk in terms of complete elliptic integrals of the first
 33 and third kinds. Gardner and Carnesale (1969), found the solid angle subtended by a circular disk by replacing the
 34 disc with a square of equal area and using a tabular correction factor. Gardner and Verghese (1971), found the
 35 solid angle subtended by a circular disc using the analytical expression for the solid angle for an n -sided regular
 36 polygon of area equal to the circular disk. Timus et. al. (2007), found a series formulation involving complete
 37 elliptic integrals for the first and second kinds for the solid angle subtended at a point by a circular disk. Conway
 38 (2010a), found an analytical solution for the solid angle subtended at any point by an ellipse using a point source
 39 radiation vector potential. Thabet, et. al. (2020), found the solid angle subtended by an ellipse with respect to a
 40 point on its axis. Conway (2010b), found the geometric efficiency for a circular detector and a linear source of
 41 arbitrary orientation and position. Abbas (2018), determined the solid angle and geometrical efficiency for a
 42 circular detector and an arbitrarily positioned line source. Ruby and Rechen (1968), computed the solid angle
 43 subtended at a disk source by a coaxial parallel-disk detector using Bessel functions of order unity. Conway (2006),
 44 generalized Ruby and Rechen's method (1968), to include cases where the detector disk and source disk are parallel
 45 but not necessarily coaxial. Thabet, et. al. (2020), computed the solid angle of a point source and a disk detector
 46 by transforming to axial geometry with an equivalent elliptical detector cross section. They used the results to
 47 evaluate the average geometrical efficiency of a coaxial disk source subtended by a circular detector using elliptical
 48 integrals. All of the methods mentioned above made use of simple geometric relationships between source and
 49 detector, as well as, various related special functions and integrals.

50

1 In this work, a general method is developed to compute the solid angle for arbitrary source and detector geometry
 2 without use of special functions or integrals. Instead of computing the area on the unit sphere to obtain the solid
 3 angle, the method introduced in this work evaluates the attitude transformation associated with an axis centered
 4 at the origin that sweeps around the perimeter of the enclosed area on the unit sphere. This method is based on
 5 Ishlinskii's theorem (1952), which states, if an axis fixed in the body, describes a closed conical surface in space, the
 6 angle of rotation of the body around this axis is equal to the integral of the projection of the angular velocity of the
 7 body onto this axis plus the solid angle of the cone enclosed. If the angular rate is zero, the rotation about the axis
 8 after it completes one circuit about the perimeter is equal to the solid angle of the enclosed cone. The attitude
 9 transformation produced by the slewing motion of the axis about the enclosed cone can be represented by a Euler
 10 rotation vector aligned with the initial orientations of the axis, which is also the final orientation of the axis. The
 11 magnitude of the Euler rotation vector is the rotation about the axis and desired solid angle of the enclosed region.
 12 Therefore, the solid angle for an arbitrary region on the surface of a unit sphere can be found by first computing
 13 the attitude transformation of the axis centered at the origin that slews about the region. The rotation angle can
 14 then be obtained from the attitude transformation. The transformation can be represented by a direction cosine
 15 matrix or a Euler rotation vector. The associated rotation angle, which is the desired solid angle, can be extracted
 16 directly from the direction cosine matrix or can be obtained as the magnitude of the Euler Rotation vector
 17 representing the transformation. The attitude transformation of the slewing motion of the axis can be found using
 18 Pivot Parameters, Patera (2017). Pivot Parameters are particularly effective in computing slewing transformations
 19 that can be viewed as great circle arcs on the unit sphere. The use of Pivot Parameters in computing solid angles
 20 of closed regions bounded by great circle arcs on the unit sphere has been presented in a related work on attitude
 21 kinematics, Patera (2020).

22
 23 Section 2 presents the method to compute the attitude transformation and associated solid angle for an arbitrary
 24 region on the unit sphere bounded by great circle arcs using the Pivot Parameter methodology. The attitude
 25 transformation is in the form of a direction cosine matrix and a simple algorithm is used to extract the associated
 26 rotation angle, which is the solid angle of the enclosed region. Section 3 presents a method to compute the solid
 27 angle of a circular or elliptical disc shaped detector with respect to a point source having arbitrary location using an
 28 n-sided polygon of equal area. Section 4 presents a method to compute the average solid angle subtended by a
 29 disk detector with respect to an arbitrary positioned line source. This method includes line sources that are coaxial
 30 to the detector's axis and to line sources having axes parallel to but not coaxial to the detector axis. Section 5
 31 presents a method to compute the average solid angle and geometrical efficiency of a disk source and coaxial disk
 32 detector. A solid angle reciprocity relationship is also introduced that is based on heat transfer considerations.
 33 Section 6 presents a method to compute the average solid angle associated with a disk source and detector system
 34 having parallel but offset axes. The first case involves an offset distance greater than the radius of the source disk
 35 and the second case involves an offset distance less than the source disk radius. Section 7 presents numerical
 36 results with a comparison to exact solid angles based on an analytical equation for a disk detector and a point
 37 source on the disk axis. Results from the proposed method are also compared to various published results
 38 involving disk shaped detectors with point, line and disk sources. Section 8 presents the conclusions.

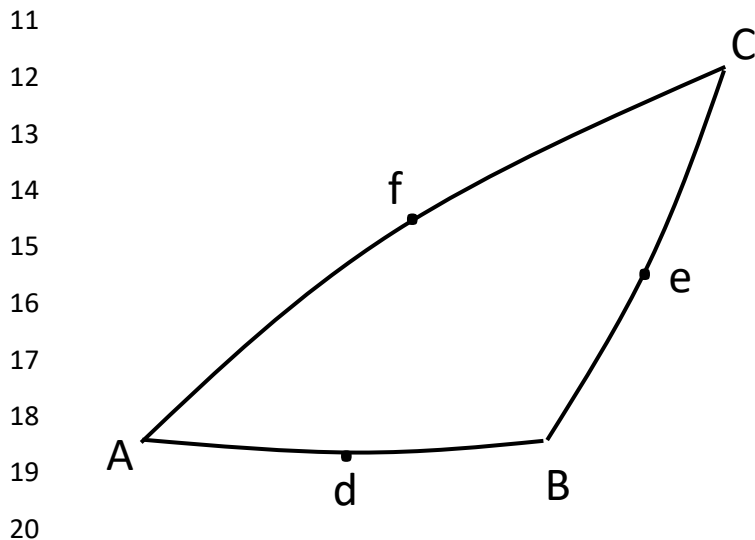
39 40 **2. Computing solid angles using Pivot Parameters**

41 A solid angle is the area on the surface of a unit sphere that is naturally parameterized using spherical coordinates
 42 in eq. (1), where the integration is over the enclosed region. The θ integration is performed to reduce the 2-
 43 dimensional integral to a 1-dimensional path integral of ϕ about the perimeter of the enclosed area in the
 44 counterclockwise direction, as shown in eq. (1).

$$45 \quad \Omega = \iint \sin(\theta) d\theta d\phi = -\oint \cos(\theta) d\phi \quad (1)$$

46 According to Ishlinskii's theorem, Ishlinskii (1952), the solid angle can also be obtained by slewing an axis around
 47 the enclosed region on the unit sphere and computing the rotation angle associated with the slewing
 48 transformation. In this application of Ishlinskii's theorem, it should be noted that there is no component of
 49 angular rate along the axis as it slews about the solid angle region. At the completion of the slewing motion, the
 50 final orientation of the axis will be exactly the same as its initial orientation before the slewing motion. However,

1 there will be a residual rotation about the axis that is given by an angle equal to the solid angle of the enclosed
 2 area on the unit sphere. It should be noted that this angle, which is generated by attitude kinematics, is not
 3 measurable by rate gyros. This new method of computing solid angle changes the problem from computing the
 4 area on a unit sphere to that of computing the attitude transformation of an axis that slews about the solid angle
 5 region on a unit sphere. The solid angle is easily obtained from its associated attitude transformation. The slewing
 6 motion can be a finite number of great circle arcs, or an infinite number of infinitesimal great circle arc segments.
 7 For solid angles associated with spherical polygons, a finite number of great circle arcs can be used to obtain the
 8 exact solid angle value. For solid angle regions bounded by smooth arcs on the unit sphere, an infinite number of
 9 infinitesimal great circle arc segments would be needed to obtain the exact solid angle value. However, the solid
 10 angle can be approximated to any degree of accuracy using a large number of great circle arcs.



21 Fig. 1. Spherical triangle defined by points a, b, c on the surface of the unit sphere is shown with the midpoints d, e,
 22 f of the great circle arc segments connecting the points.

23 Consider the solid angle of a spherical triangle defined by points a, b, c located on the surface of a unit sphere
 24 shown in Fig. 1. An axis with one end located at the origin of the sphere moves its tip from a to b to c back to a,
 25 thereby completing one circuit about the spherical triangle. The first great circle arc segment links point a to point
 26 b, and has an associated attitude transformation given by $U(a, b)$. The Euler rotation vector associated with this
 27 transformation is directed normal to the great circle arc and has no component along the axis at any orientation of
 28 the axis during its slewing motion. Slewing motion along a single great circle arc does not produce rotation about
 29 the axis. The transformation produced by the axis after it has moved about the spherical triangle is given by the
 30 product of the transformations associated with the three great circle arc segments in sequence, as shown in eq.
 31 (2).

$$32 \quad U = U(a, b) U(b, c) U(c, a) \quad (2)$$

33 The attitude transformation associated with each great circle arc segment can be readily computed using the Pivot
 34 Parameter formulation, Patera (2017). In the Pivot Parameter method, a rotation is specified by two Pivot
 35 Vectors located in the rotation plane centered at the origin of the coordinate system. The angle between the Pivot
 36 Vectors is one half of the desired rotation angle. A rotation of 180 degrees about the first Pivot Vector followed by
 37 a rotation of 180 degrees about the second Pivot Vector achieves the desired rotation, which propagates each
 38 Pivot Vector along a segment of a great circle arc that represents the desired rotation. Let d, e, and f be the
 39 midpoints of segments a-b, b-c, and c-a, respectively. A 180 degree rotation about a followed by a 180 degree
 40 rotation about d results in the desired great circle arc slewing from a to b, as shown in eq. (3). The same

1 transformation can be achieved using a 180 degree rotation about d followed by a 180 rotation about b, as shown
2 in eq. (3).

$$3 \quad U(\mathbf{a}, \mathbf{b}) = \mathbf{R}(\mathbf{a}, \mathbf{180}) \mathbf{R}(\mathbf{d}, \mathbf{180}) = \mathbf{R}(\mathbf{d}, \mathbf{180}) \mathbf{R}(\mathbf{b}, \mathbf{180}) \quad (3)$$

4 The rotation transformation defined by a rotation about \mathbf{r} of angle α is given by the direction cosine matrix in eq.
5 (4), Patera (2010), where $C=\cos(\alpha)-1$ and $S=\sin(\alpha)$.

$$6 \quad \mathbf{R}(\mathbf{r}, \alpha) = \begin{pmatrix} 1 + (r_x^2 + r_y^2)C & -(r_x r_y C + r_z S) & r_y S - r_x r_z C \\ r_z S - r_x r_y C & 1 + (r_x^2 + r_z^2)C & -(r_z r_y C + r_x S) \\ -(r_x r_z C + r_y S) & r_x S - r_y r_z C & 1 + (r_x^2 + r_y^2)C \end{pmatrix} \quad (4)$$

7 When $\alpha=180$ degrees, eq. (4) reduces to eq. (5), which defines $\boldsymbol{\psi}(\mathbf{r})$ and $\mathbf{R}(\mathbf{r}, \mathbf{180})$. Note that the transformation is
8 orthonormal, since \mathbf{r} is a unit vector.

$$9 \quad \mathbf{R}(\mathbf{r}, \mathbf{180}) = \boldsymbol{\psi}(\mathbf{r}) = \begin{pmatrix} 2r_x^2 - 1 & 2r_x r_y & 2r_x r_z \\ 2r_x r_y & 2r_y^2 - 1 & 2r_z r_y \\ 2r_x r_z & 2r_z r_y & 2r_z^2 - 1 \end{pmatrix} \quad (5)$$

10 Using eq. (5) in eq. (3), one obtains eq. (6).

$$11 \quad U(\mathbf{a}, \mathbf{b}) = \boldsymbol{\psi}(\mathbf{a}) \boldsymbol{\psi}(\mathbf{d}) = \boldsymbol{\psi}(\mathbf{d}) \boldsymbol{\psi}(\mathbf{b}) \quad (6)$$

12 The same procedure can be used to obtain the other two great circle arc transformations given by eqs. (7) & (8).

$$13 \quad U(\mathbf{b}, \mathbf{c}) = \boldsymbol{\psi}(\mathbf{b}) \boldsymbol{\psi}(\mathbf{e}) = \boldsymbol{\psi}(\mathbf{e}) \boldsymbol{\psi}(\mathbf{c}) \quad (7)$$

$$14 \quad U(\mathbf{c}, \mathbf{a}) = \boldsymbol{\psi}(\mathbf{c}) \boldsymbol{\psi}(\mathbf{f}) = \boldsymbol{\psi}(\mathbf{f}) \boldsymbol{\psi}(\mathbf{a}) \quad (8)$$

15 Two rotations can be combined by joining their associated great circle arc segments at their intersection points.
16 Using eqs. (6) & (7), one finds the combined transformation from a to c, as shown in eq. (9). Notice that the two
17 180 rotations about the axis at point b results in a 360 degree rotation or no rotation at all.

$$18 \quad U(\mathbf{a}, \mathbf{b}) U(\mathbf{b}, \mathbf{c}) = \boldsymbol{\psi}(\mathbf{d}) \boldsymbol{\psi}(\mathbf{b}) \boldsymbol{\psi}(\mathbf{b}) \boldsymbol{\psi}(\mathbf{e}) = \boldsymbol{\psi}(\mathbf{d}) \boldsymbol{\psi}(\mathbf{e}) \quad (9)$$

19 The complete transformation around the spherical triangle, as given by eq. (2) can be obtained using eqs. (8) & (9),
20 as shown in eq. (10).

$$21 \quad U = U(\mathbf{a}, \mathbf{b}) U(\mathbf{b}, \mathbf{c}) U(\mathbf{c}, \mathbf{a}) = \boldsymbol{\psi}(\mathbf{d}) \boldsymbol{\psi}(\mathbf{e}) \boldsymbol{\psi}(\mathbf{f}) \boldsymbol{\psi}(\mathbf{a}) \quad (10)$$

22 A similar equation can be created for a spherical quadrilateral with the midpoint of the fourth side given by g, as
23 shown in eq. (11).

$$24 \quad U = \boldsymbol{\psi}(\mathbf{d}) \boldsymbol{\psi}(\mathbf{e}) \boldsymbol{\psi}(\mathbf{f}) \boldsymbol{\psi}(\mathbf{g}) \quad (11)$$

25 For any polygon having an even number of sides, the close loop transformation of the axis around the solid angle
26 region is given by the product of the transformations corresponding to 180 degree rotations about the midpoints
27 of the sides in the sequence corresponding to the axis trajectory. If the number of sides of the spherical polygon is
28 odd, an additional final rotation of 180 degrees about the initial point is required to complete the transformation,
29 as is shown in eq. (10). This method can be extended to any number of connected great circle arc segments that
30 form enclosed regions on the unit sphere. The solid angle can also be found for any region on the surface of a unit
31 sphere enclosed by a continuous curve, since the curve can be approximated to any degree of accuracy with a
32 large number of infinitesimal great circle arc segments. The attitude transformation associated with the great
33 circle arc segments can be computed using Pivot Parameters, as shown, and the associated rotation angle or solid
34 angle, can be extracted from the direction cosine matrix. Alternatively, the solid angle can be found as the

1 magnitude of the Euler rotation vector corresponding to the transformation. Note that the Euler rotation vector
2 aligns with the initial orientation of the axis.

3 The rotation angle can be extracted from the direction cosine matrix by first computing the trace of the matrix,
4 which is the sum of the diagonal elements, as shown in eq. (12).

$$5 \quad \text{Trace} = U(1,1) + U(2,2) + U(3,3) \quad (12)$$

6 The solid angle, Ω , can be found using eq. (13).

$$7 \quad \Omega = \cos^{-1} \left[\frac{\text{trace} - 1}{2} \right] \quad (13)$$

8 The components of the Euler rotation vector, V , can be found using eq. (14), once Ω is obtained from eq. (13).

$$9 \quad V(1) = [U(3,2) - U(2,3)] \frac{\Omega}{2 \sin(\Omega)}$$

$$10 \quad V(2) = [U(1,3) - U(3,1)] \frac{\Omega}{2 \sin(\Omega)} \quad (14)$$

$$11 \quad V(3) = [U(2,1) - U(1,2)] \frac{\Omega}{2 \sin(\Omega)}$$

12 Since the Ω can be as large as 2π but the largest magnitude of Ω that can be obtained by eq. (13) is only π , the sign
13 of $V(3)$ can be used to determine the true value of Ω . If $V(3) < 0$, the solid angle is given by eq. (13). If $V(3) > 0$, the
14 solid angle is given by eq. (15). This logic depends on the details of the geometry.

$$15 \quad \Omega = 2\pi - \cos^{-1} \left[\frac{\text{trace} - 1}{2} \right] \quad (15)$$

16

17

18 3. The solid angle subtended by a circular or elliptical disk

19 The first application of the general method of computing solid angle is that of a point source and a circular disk
20 detector. It should be noted that Garner and Carnesale (1969), addressed this problem by replacing the circular
21 disk with a square of equal area. Their method worked well but required use of a correction factor table to be
22 accurate in cases of interest. The method was expanded by Garner and Verghese (1971), who replaced the circular
23 disk with an n-sided regular polygon of area equal to that of the disk. They found that a 36-sided regular polygon
24 was sufficient to obtain accurate results. The general method of computing solid angle, proposed in this work, also
25 replaces the circular disk with an n-sided regular polygon. The first step is to replace the radius of the disk with a
26 larger disk that encompasses the n-sided regular polygon of equal area. If R_0 is the radius of the original disk, then
27 the radius of the enlarged disk is given by eq. (16), where n is the number of sides selected.

$$28 \quad R = R_0 \sqrt{\left[\frac{\pi}{n \sin\left(\frac{\pi}{n}\right) \cos\left(\frac{\pi}{n}\right)} \right]} \quad (16)$$

29 The regular polygon is defined by vertices ordered in the counterclockwise direction and labeled by index k that
30 ranges from 1 to $n+1$. Let $a(k)$ be the x component of the k^{th} vertex and $b(k)$ the y component of the k^{th} vertex, as
31 shown in eq. (17). Notice that $a(1) = a(n+1)$ and $b(1) = b(n+1)$.

$$32 \quad a(k) = R \cos \left[\frac{2\pi(k-1)}{n} \right] \quad , \quad b(k) = R \sin \left[\frac{2\pi(k-1)}{n} \right] \quad (17)$$

33 Adjacent vertices are connected by straight line segments in the x-y plane. The midpoints of the line segments are
34 given by eq. (18), where m ranges from 1 to n . Note that $z(m) = 0$ for all m , since the polygon is in the x-y plane.

$$x(m) = [a(m+1) + a(m)]/2, \quad y(m) = [b(m+1) + b(m)]/2 \quad (18)$$

The source, \mathbf{s} , is placed anywhere in the upper hemisphere for convenience so that sequential axis locations are defined by eq. (19), where $r(m, i)$ defines the coordinates of the tip of the line segment with respect to the source. Note that there is no restriction of the location of \mathbf{s} , such as, being on the axis of the disk.

$$r(m, 1) = x(m) - s(1), \quad r(m, 2) = y(m) - s(2), \quad r(m, 3) = -s(3) \quad (19)$$

For simplicity, we choose n to be an even number, which results in an even number of axis orientations that define the midpoint of the n -line segments. Each vector, $\mathbf{r}(\mathbf{m})$, defines the location of the m^{th} midpoint with respect to the source and must be unitized before it can be used in eq. (5). If $n = 4$, the attitude transformation associated with the axis slewing about the 4-sided regular polygon is given by eq. (20), where $\mathbf{r}(\mathbf{m})$ are the unit vectors.

$$\mathbf{U} = \psi[\mathbf{r}(1)] \psi[\mathbf{r}(2)] \psi[\mathbf{r}(3)] \psi[\mathbf{r}(4)] \quad (20)$$

Eq. (20) can be generalized to an n -sided regular polygon, as given by eq. (21).

$$\mathbf{U} = \prod_{m=1}^n \psi[\mathbf{r}(\mathbf{m})] \quad (21)$$

Once the transformation is obtained for the closed path slewing motion of the axis about the solid angle region, eqs. (13) and (14) are used to obtain the value of the solid angle. Note that although the polygon is located in the x - y plane, the normalized vertices are located on the surface of a unit sphere centered at the source. The solid angle region is the area on the unit sphere defined by the normalized vectors that define the vertices on the unit sphere. Eq. (21) is the exact transformation associated with the slewing motion of the axis about the polygon region. By choosing a large enough n , eq. (21) approximates the transformation of the axis about the original disk in the x - y plane to any desired degree of accuracy within the limits of numerical processing errors.

The solid angle of an elliptical disk can be obtained by adjusting the x and y components in eq. (17). If the semi-major axis and semi-minor axis are given by A and B respectively, then eq. (17) becomes eq. (22).

$$a(k) = A \cos \left[\frac{2\pi(k-1)}{n} \right], \quad b(k) = B \sin \left[\frac{2\pi(k-1)}{n} \right] \quad (22)$$

With the eq. (22) replacing eq. (17), the processing to compute the solid angle is exactly the same as for the circular disk. This method does not require the source to be coaxial with the disk as does Thabet, et. al. (2020), who computed the solid angle of a point source and a disk detector by transforming to axial geometry with an equivalent elliptical detector cross section. The general method of computing solid angle applies to any location of the source, as long as eq. (22) is used in place of eq. (17).

4. Average solid angle subtended by a disk detector with respect to an arbitrary linear source

The general method to compute solid angle developed in Section 3 can be used to find the average solid angle for a disk detector with respect to a linear source. The linear source is represented by a discrete number of point sources distributed uniformly along its length. Let the linear source extend from $\mathbf{L1}(\mathbf{i})$ to $\mathbf{L2}(\mathbf{i})$, where the index, i , represents the x , y , and z components of the location. The linear source is represented by n point sources separated by $d\mathbf{L}$, as given in eq. (23). The location of each point source is given by eq. (24) to provide a uniform distribution across the length of the source.

$$d\mathbf{L} = (\mathbf{L2} - \mathbf{L1})/n \quad (23)$$

$$\mathbf{S}(\mathbf{k}) = \mathbf{L1} + k d\mathbf{L} - d\mathbf{L}/2 \quad (24)$$

The k^{th} point source location is used in the algorithm presented in Section 3 to generate the associated solid angle, $G(k)$, as given in eq. (25).

$$G(k) = \Omega[\mathbf{S}(\mathbf{k})] \quad (25)$$

1 The average solid angle for the linear source can be found by simply averaging the values of $G(k)$, as shown in eq.
2 (26).

$$3 \quad \Omega = \frac{1}{n} \sum_{k=1}^n G(k) \quad (26)$$

4 Since, the orientation of the linear source does not have to be coaxial to the detector axis or even parallel to the
5 detector axis, eq. (26) is a general result.

6 The numerical integration method represented in eq. (26) can be enhanced to improve accuracy by employing a
7 two point Gaussian integration algorithm. In the Gaussian integration algorithm, eq. (24) is replaced with eq. (27),
8 where the single evaluation of each $\mathbf{S}(\mathbf{k})$ is replaced by two evaluations, $\mathbf{S1}(\mathbf{k})$ and $\mathbf{S2}(\mathbf{k})$.

$$9 \quad \mathbf{S1}(\mathbf{k}) = \mathbf{L1} + k \mathbf{dL} - \frac{\mathbf{dL}(1+1/\sqrt{3})}{2}, \quad \mathbf{S2}(\mathbf{k}) = \mathbf{L1} + k \mathbf{dL} - \frac{\mathbf{dL}(1-1/\sqrt{3})}{2} \quad (27)$$

10 In a similar fashion, G in eq. (25) was replaced by $G1$ and $G2$ in eq. (28).

$$11 \quad G1(k) = \Omega[\mathbf{S1}(\mathbf{k})], \quad G2(k) = \Omega[\mathbf{S2}(\mathbf{k})] \quad (28)$$

12 The average solid angle is obtained by replacing eq. (26) with eq. (29).

$$13 \quad \Omega = \frac{1}{2n} \sum_{k=1}^n [G1(k) + G2(k)] \quad (29)$$

14 The associated geometrical efficiency, GE , which is the solid angle divided by 4π , is given by eq. (30).

$$15 \quad GE = \Omega/4\pi = \frac{1}{8n\pi} \sum_{k=1}^n [G1(k) + G2(k)] \quad (30)$$

16

17 5. Average solid angle of a disk detector with respect to a coaxial disk source

18 The average solid angle subtended by a coaxial disk detector with respect to a coaxial disk source can be found
19 using the results of Section 4, where the linear source is replaced with radial points that extend from the center of
20 the disk source to a point on the perimeter of the disk source. In this case, $\mathbf{L1}$ is at the center of the disk source
21 and $\mathbf{L2}$ is at any point on the perimeter of the disk source. The solid angle for the k^{th} point between $\mathbf{L1}$ and $\mathbf{L2}$ is
22 given by eq. (25). The average solid angle for the disk source can be found by the weighted average of $G(k)$, as
23 given in eq. (31), where dL is the magnitude of \mathbf{dL} , as given by eq. (23).

$$24 \quad \Omega = \frac{2}{(L2-L1)^2} \sum_{k=1}^n G(k) |k \mathbf{dL} - \mathbf{dL}/2| dL \quad (31)$$

25 Note that eq. (31) can also be written, as shown in eq. (32).

$$26 \quad \Omega = \frac{2}{(L2-L1)^2} \sum_{k=1}^n G(k) |\mathbf{S}(\mathbf{k}) - \mathbf{L1}| dL \quad (32)$$

27 Eq. (31) can be understood more easily by considering the average solid angle subtended by the disk detector over
28 the disk source using a continuous integral average, as shown in eq. (33), where $G(r)$ is the associated continuous
29 function and ρ is the radius of the disk source. Notice that ρ is given by the absolute value of $\mathbf{L2} - \mathbf{L1}$.

$$30 \quad \Omega = 2/\rho^2 \int_0^\rho G(r) r dr \quad (33)$$

31 The geometrical efficiency corresponding to eq. (33) is given by eq. (34).

$$32 \quad GE = \Omega/4\pi = \frac{1}{2\pi \rho^2} \int_0^\rho G(r) r dr \quad (34)$$

1 The numerical integration method in eq. (31) was made more accurate by employing a two point Gaussian
 2 integration algorithm, as presented in Section 4. As before, $\mathbf{S1}$ and $\mathbf{S2}$ are defined by eq. (27) and the respective
 3 solid angles are defined by eq. (28). The average solid angle can be found by replacing eq. (32) with eq. (35).

$$4 \quad \Omega = \frac{1}{(L2-L1)^2} \sum_{k=1}^n [G1(k)|\mathbf{S1}(k) - \mathbf{L1}| + G2(k)|\mathbf{S2}(k) - \mathbf{L1}|] dL \quad (35)$$

5 Consider the case where the source and the disk are both black body radiators, which having emissivity and
 6 absorptivity values of 1, and are in thermal equilibrium with each other. In this case, the infrared radiation
 7 emitted by the source and absorbed by the detector is exactly equal to the infrared radiation emitted by the
 8 detector and absorbed by the source. Since the total power radiated by source and detector is proportional the
 9 respective surface areas, the heat balance equation between source and detector is given by eq. (36), where R is
 10 the radius of the circular detector and ρ is the radius of the circular source.

$$11 \quad \pi \rho^2 \Omega_s = \pi R^2 \Omega_R \quad (36)$$

12 The average solid angle of the detector as observed at the source is given by Ω_s and the average solid angle of the
 13 source as observed at the detector is given by Ω_R . Therefore, the value of Ω_R can be used to find the value of Ω_s , as
 14 shown in eq. (37).

$$15 \quad \Omega_s = \frac{R^2}{\rho^2} \Omega_R \quad (37)$$

16 This reciprocity relationship may be useful in cases where reversing the rolls of source and detector facilitate
 17 computation or improve computation accuracy.

18 6. Average solid angle of a disk detector with respect to a parallel offset disk source

19 The average solid angle can be calculated for the case of a circular disk source and detector system having parallel
 20 axes that are offset from coaxial alignment. The problem can be solved by considering a larger coaxial disk source
 21 having a radius equal to the offset distance plus the radius of the original offset disk source, as shown in Fig. 2.

22

23

24

25

26

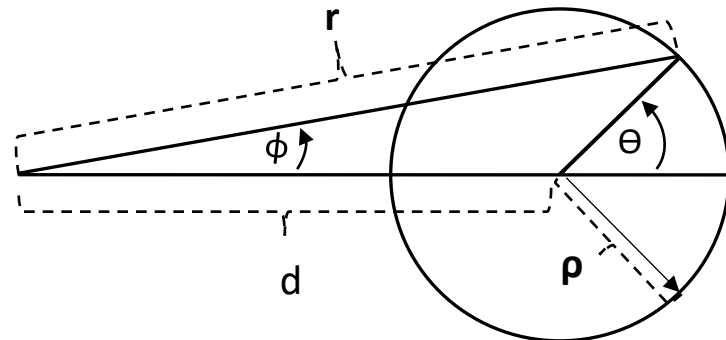
27

28

29

30

31



31 Fig. 2. Circular integration region when d is greater than ρ .

32

33 In this case, the integration region is not over the entire enlarged disk source, but just the original disk source. In
 34 the situation shown in Fig. 2, the offset distance is larger than the radius of the source. The distance from the
 35 detector axis in the x-y plane to the perimeter of the disk source is given by r, where r is related to d, ρ , and Θ by
 36 eq. (38.)

$$r^2 = [d + \rho \cos(\theta)]^2 + \rho^2 \sin^2(\theta) \quad (38)$$

In eq. (38), d is the shift distance, ρ is the radius of the source disk and θ is the angle defined in Fig. 2. By taking the derivative of eq. (38), one finds the relationship between dr and $d\theta$, as shown in eq. (39).

$$r dr = -\rho d \sin(\theta) d\theta \quad (39)$$

The integral of the solid angle over the disk source region parameterized by r makes use of the coaxial symmetry, as shown in eq. (40). The integration parameter is changed from r to a θ using eq. (38) and eq. (39), as shown in eq. (40). $G(r)$ is a function of θ through eq. (38), which relates r and θ .

$$I = \int_{d-\rho}^{d+\rho} 2 G(r) \phi r dr = -2 \rho d \int_{\pi}^0 G(\theta) \phi \sin(\theta) d\theta = 2 \rho d \int_0^{\pi} G(\theta) \phi \sin(\theta) d\theta \quad (40)$$

Note that ϕ is a function of θ , since, at each value of θ , ϕ is obtained as the inverse of $\tan(\phi)$, as given by eq. (41). Since d is greater than ρ , the value of ϕ is between 0 and 90 degrees.

$$\phi = \tan^{-1} \left[\frac{\rho \sin(\theta)}{d + \rho \cos(\theta)} \right] \quad (41)$$

Eq. (40) can be integrated numerically using the two-point gaussian algorithm with $\Delta\theta = \pi/n$ and θ_1 and θ_2 defined in eq. (42).

$$\theta_1(k) = k \Delta\theta - \frac{\Delta\theta(1+\sqrt{3})}{2}, \quad \theta_2(k) = k \Delta\theta - \frac{\Delta\theta(1-\sqrt{3})}{2} \quad (42)$$

Using the definitions in eqs. (43) - (45), one finds the numerical integral of eq. (40), as shown in eq. (46).

$$G_1(k) = \Omega[\theta_1(k)], \quad G_2(k) = \Omega[\theta_2(k)] \quad (43)$$

$$\phi_1(k) = \phi[\theta_1(k)], \quad \phi_2(k) = \phi[\theta_2(k)] \quad (44)$$

$$\sin_1(k) = \sin[\theta_1(k)], \quad \sin_2(k) = \sin[\theta_2(k)] \quad (45)$$

$$I = \frac{\rho d}{n} \sum_{k=1}^n [G_1(k) \phi_1(k) \sin_1(k) + G_2(k) \phi_2(k) \sin_2(k)] \Delta\theta \quad (46)$$

The average solid angle over the disk source for the continuous integral is found by dividing eq. (40) by the area of the disk source as given by eq. (47). Therefore, the numerical summation in eq. (46) must be divided by the area of the disk source to obtain the average solid angle, as given by eq. (48).

$$\langle \Omega \rangle = \frac{I}{\pi \rho^2} = \frac{2 \rho d \int_0^{\pi} G \phi \sin(\theta) d\theta}{\pi \rho^2} \quad (47)$$

$$\langle \Omega \rangle = \frac{d}{\pi n \rho} \sum_{k=1}^n [G_1(k) \phi_1(k) \sin_1(k) + G_2(k) \phi_2(k) \sin_2(k)] \Delta\theta \quad (48)$$

The second situation shown in Fig. 3, has the offset distance smaller than the radius of the disk source. Once again, we consider a larger coaxial disk source having radius equal to d plus ρ . In this case, eq. (38) and eq. (39) are replaced with eq. (49) and eq. (50), respectively.

$$r^2 = [\rho \cos(\theta) - d]^2 + \rho^2 \sin^2(\theta) \quad (49)$$

$$r dr = \rho d \sin(\theta) d\theta \quad (50)$$

The integral of the enlarged coaxial disk source, I_E , minus the original shifted disk source, I_S , is given by I , as shown in eq. (51), where eq. (50) has been used to change the integration parameter to θ .

$$I = I_E - I_S = \int_{\rho-d}^{d+\rho} 2 G \phi r dr = 2 \rho d \int_0^{\pi} G \phi \sin(\theta) d\theta \quad (51)$$

1 Although eq. (51) has the same form as eq. (40), the integrand is different, since eq. (41) is replaced by eq. (52),
 2 when determining ϕ from Θ . Since ρ is greater than d in eq. (52), $\tan(\phi)$ can be negative and the value of ϕ is
 3 between 0 and 180 degrees. In addition, the replacement of eq. (38) with eq. (49) changes the value of G in the
 4 integrand.

$$5 \quad \phi = \tan^{-1} \left[\frac{\rho \sin(\theta)}{\rho \cos(\theta) - d} \right] \quad (52)$$

6 Eq. (51) is evaluated numerically using the two point gaussian integration algorithm, as given by eq. (46) but with
 7 the appropriate changes to the integrand. I_E is evaluated using the method of Section 5 and is given by eq. (53).

$$8 \quad I_E = 2\pi \int_0^{\rho+d} G r dr \quad (53)$$

9 Once values for I and I_E are obtained from eq. (51) and eq. (53), the average solid angle over the shifted disk source
 10 is obtained by eq. (54). Therefore, one doesn't evaluate the average solid angle over the shifted source directly,
 11 since it is easily obtained indirectly using I and I_E . The related geometrical efficiency is obtained by dividing eq. (54)
 12 by 4π , as given by eq. (55).

$$13 \quad \langle \Omega \rangle = \frac{I_S}{\pi \rho^2} = \frac{I_E - I}{\pi \rho^2} \quad (54)$$

$$14 \quad GE = \frac{I_S}{4\pi^2 \rho^2} = \frac{I_E - I}{4\pi^2 \rho^2} \quad (55)$$

15

16

17

18

19

20

21

22

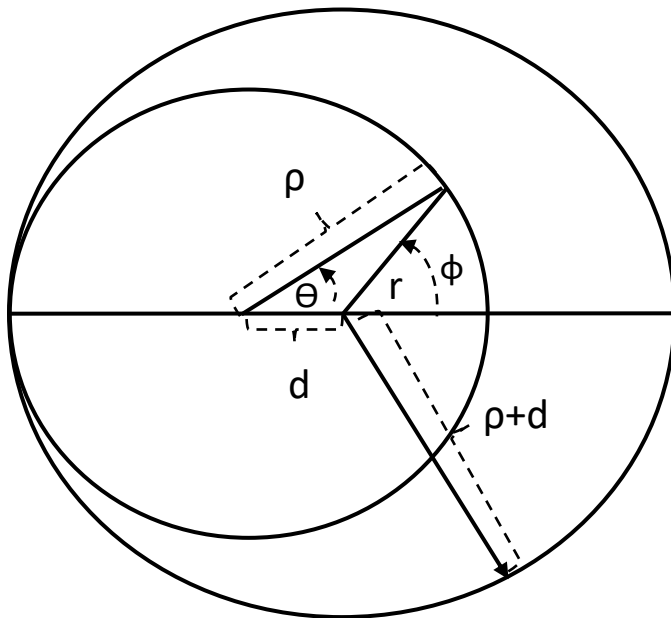
23

24

25

26

27



28 Fig. 3. Integration region is between the circles when d is less than ρ .

29 7. Numerical results

30 The new method to compute solid angle was implemented in several computer simulations to demonstrate its
 31 performance. Results of the new method were first compared to the exact solution of a simple known case
 32 involving a point source located on the axis of a disk detector. For a point source located at a distance h along the
 33 axis of a disk having radius R , the solid angle is given by eq. (56).

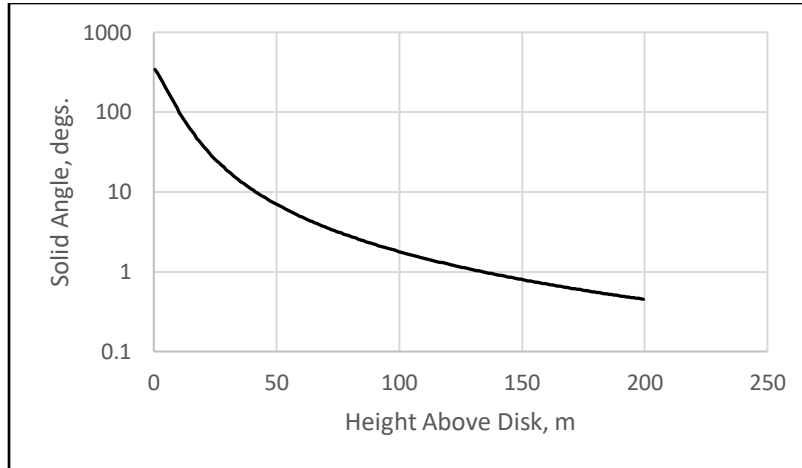
1

$$\Omega = 2\pi \left[1 - \frac{h}{\sqrt{R^2 + h^2}} \right] \quad (56)$$

2 Figure 4 shows the solid angle obtained using eq. (56), when $R = 10$ and h ranges from 0 to 200. The solid angle
 3 was also computed using the general method with a 360-sided regular polygon in place of the disk. The polygon
 4 was expanded to have an area equal to that of the disk. Figure 5 shows the percent difference between the solid
 5 angle of the polygon, which was found using the general method, and the solid angle of the disk using eq. (56).
 6 Note that the solid angle of the polygon is exact except for numerical processing errors. Therefore, the error in Fig.
 7 5 shows how well the polygon's solid angle represents that of the disk. When the number of sides of the polygon
 8 was increased from 360 to 800, it more accurately represented the circular disk and the percent error decreased,
 9 as shown in Fig. 5. The noisy values in Fig. 5 are caused by numerical processing error at larger values of h . The
 10 extremely small error displayed in Fig. 5 indicates that the general method using the polygon is highly accurate.
 11 The advantage of the general method is that the point source can be located at any point and does not have to be
 12 on the axis of the disk, as required by eq. (56).

13

14



15

16 Fig. 4. Exact solid angle of a disk having radius or 10 meters with respect to a point above a disk along its axis.

17

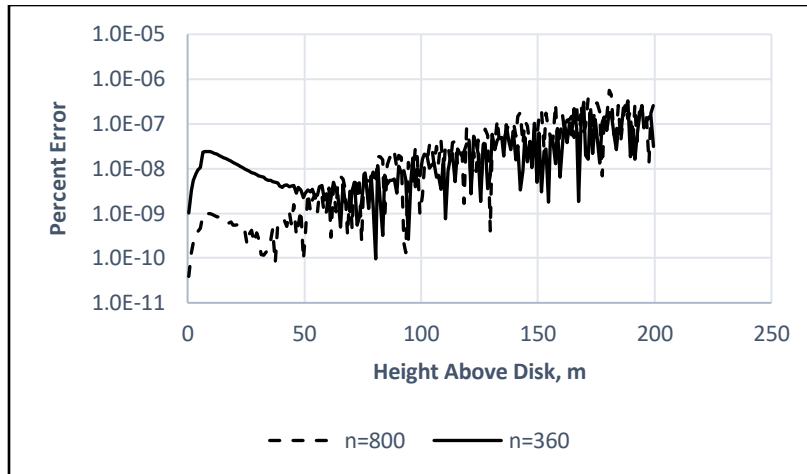
18

19

20

21

22



1
2 Fig. 5. Percent error of the general method when using 360-sided and 800-sided polygons to represent the
3 circular disk.

4

5 7.1 Point source on the axis of an elliptical disk detector

6 The general method can be modified easily to compute the solid angle of an elliptical disk with respect to a point
7 source along the axis normal to the plane of the disk, as presented in Section 3. Let A and B be the semi-major axis
8 and semi-minor axes of the ellipse, respectively. In this case, eq. (17) is replaced with eq. (22) and the remainder
9 of the processing is the same.

10 Table 1. Solid angle comparison for an elliptical detector with point source on the detector axis

Case #	A	B	h	Conway (2010a)	Thabet, et. al. (2020)	General Method (n=360)
1	2	1	0.01	6.2347447	6.2346390	6.2347447
2	2	1	0.5	4.0425592	4.0423850	4.0425592
3	2	1	10	0.0616819	0.0616804	0.0616819
4	1000	1	1	3.1415778	3.1414940	3.1416101 [3.1415778, (n = 2200)]
5	100	1	1	3.1405637	3.1404830	3.1405643 [3.1405637, (n = 500)]
6	1	0.99	1	1.8291325	1.8290270	1.8291325
7	1	0.2	1	0.4724316	0.4724257	0.4724316
8	1	0.01	1	0.0239619	0.0239632	0.0239619
9	1	0.001	1	0.0023963	0.0023972	0.0023963

11

12 The results using the general method was compared to published results, Thabet, et. al. (2020) in Table 1, which
13 includes results from Conway (2010a). The results of the proposed general method, when rounded down to seven
14 digits to the right of the decimal point, agreed with the results of Conway (2010a). All cases used a 360-sided
15 polygon. The number of sides for case #4 was increased to 2200, as shown in parentheses, to match Conway's
16 result exactly. The number of sides for case #5 was increased to 500 to match Conway's result exactly. Although
17 cases #4 and #5 are numerically stressful cases, the general method proposed in this work can achieve any desired
18 degree of accuracy by increasing the number of sides of the polygon. The only limitation is numerical processing
19 error.

20 The general method can also handle cases where the point source is not located on the axis of the elliptical
21 detector. Table 2 shows that the general method, while using a 360-sided polygon, produces results in exact

1 agreement to those of Conway (2010a). The results in Table 2 show that the general method is valid for sources
2 located anywhere with respect to the elliptical detector.

3 Table 2. Solid angle for an elliptical detector with respect to a point source located at (p, q, h)

Case #	A	B	p	q	h	Conway (2010a)	General Method (n=360)
1	1.5	1.0	0.6	0.5	0.1	5.4932906	5.4932906
2	1.5	1.0	0.6	0.5	2.52	0.5690505	0.5690505
3	1.5	1.0	0.6	0.5	10.0	0.0461472	0.0461472
4	1.0	4.0	2.0	0.5	0.1	0.1104206	0.1104206
5	1.0	4.0	0.1	4.0	5.0	0.2589691	0.2589691
6	2.0	1.0	1.0	0.5	1.0	1.9450789	1.9450789
7	2.0	1.0	5.0	1.0	1.0	0.0547517	0.0547517
8	3.0	1.0	1.0	0.5	0.5	3.6792113	3.6792113
9	5.0	1.0	1.0	0.5	0.5	3.9166119	3.9166119
10	1.1	1	1	0.9	2.0	0.4744215	0.4744215

4

5 7.2 Line source parallel to the axis of a circular disk detector

6 The average solid angle subtended by a disk detector with respect to a line source parallel to the disk axis was
7 computed using the method of Section 4. In Section 4 the points were distributed uniformly over the length of the
8 line source and the associated solid angles were averaged to obtain the average solid angle subtended by the disk
9 detector. The method was then enhanced to improve accuracy by employing a two point Gaussian integration
10 algorithm. The algorithm was applied to computing the geometrical efficiency of a line source along the axis of a
11 disk detector and the results were compared to similar results published by Abbas (2018), in Table 3, which also
12 contains results from Conway (2010b).

13 Table 3. Geometrical efficiency for a coaxial line source of length 2a

Case #	R	h	a	Conway (2010b)	Abbas (2018)	General Method (n=360)
1	10	5	3	0.2826492	0.2826492	0.2826492
2	10	5	5	0.2928932	0.2928932	0.2928932
3	105	5	5	0.4999750	0.4999750	0.4999750
4	10	1	1	0.4504902	0.4504902	0.4504902
5	10	0.1	0.1	0.4950005	0.4950005	0.4950005
6	10	100	2	0.0024824	0.0024824	0.0024824
7	10	100	100	0.0243754	0.0243754	0.0243754
8	5	5	5	0.1909830	0.1909830	0.1909830
9	10	10	2	0.1482186	0.1482186	0.1482186

14

15 In Table 3, R is the radius of the circular disk detector, h is the distance along the detector axis corresponding to
16 the midpoint of the line source and a is one half of the length of the line source. All the results were obtained
17 using a 360-sided polygon and were rounded down to seven digits to the right of the decimal point to provide
18 uniformity, although the general method agreed with the published results to many more digits.

19 The general method was also applied to computing the geometrical efficiency of a line source parallel to the axis of
20 the circular disk detector, but not coaxial to the disk axis. The results were in perfect agreement with similar
21 published results of Abbas (2018), and Conway (2010b), as shown in Table 4. The notation in Table 4 is the same

1 as that of Table 3 but Table 4 has the additional parameter, d , which is the distance that the parallel line source
 2 was shifted from the axis of the disk detector. All results were rounded down to seven digits to the right of the
 3 decimal to maintain uniformity.

4 Table 4. Geometrical efficiency for a parallel line source shifted by d and of length $2a$

Case #	R	d	h	a	Conway (2010b)	Abbas (2018)	General Method (n=360)
1	10	1	6	1	0.2424075	0.2424075	0.2424075
2	10	1	6	6	0.2650418	0.2650418	0.2650418
3	50	1	6	6	0.4408232	0.4408232	0.4408232
4	1000	1	6	6	0.4970001	0.4970001	0.4970001
5	5	1	5	4	0.1726042	0.1726042	0.1726042
6	5	10	5	4	0.0226308	0.0226308	0.0226308
7	20	5	1	1	0.4738339	0.4738339	0.4738339
8	20	5	10	1	0.2697133	0.2697133	0.2697133
9	20	5	40	1	0.0519778	0.0519778	0.0519778

5

6 7.3 Circular disk source coaxial to a disk detector

7 The geometrical efficiency associated with a coaxial disk source with respect to a circular disk detector was
 8 computed according to Section 5 and compared to published results Selim and Abbas (1994) in Table 5.

9 Table 5. Solid angle for coaxial circular detector of radius R separated by h from a circular source of radius ρ

Case #	R	h	ρ	Selim and Abbas (1994)	General Method (n=360)
1	1	10	1	0.03097	0.0309543
2	1	10	4	0.02792	0.0279254
3	1	10	7	0.02309	0.0230928
4	1	10	10	0.01836	0.0183614
5	12	10	12	1.75641	1.7564276
6	12	10	15	1.52114	1.5211577
7	12	10	17	1.36655	1.3665614
8	12	10	19	1.22193	1.2219275
9	28	10	23	3.60777	3.6078341
10	28	10	25	3.47289	3.4729432
11	28	10	28	3.23495	3.2349867
12	28	10	30	3.05770	3.0577027

10

11 Although the published results in Table 5 include only five digits to the right of the decimal point, the general
 12 method included seven digits. It is evident in Table 5, that some of the published results are not as accurate as
 13 that of the general method, which used a 360-sided polygon. If such accurate results are not essential, the number
 14 of sides of the representative polygon can be reduced.

15 The general method was tested against results of a more recent publications, Vega-Carrillo (1996), Conway (2006),
 16 and Thabet, et. al. (2020), as shown in Table 6. In this case, only four digits to the right of the decimal point were
 17 included in the published results, except for Conway's results, which included seven digits. Results of the general
 18 method agree exactly with Conway's results in all cases. Cases #6, #8, and #9 have values from the general
 19 method that when rounded to only four digits agree with results of either Vega-Carrillo (1996), or Thabet, et. al.

1 (2020) or both. These results indicate that round-off differences may have contributed to the discrepancy in some
2 of the published results.

3 Table 6. Geometrical efficiency for a coaxial circular detector of radius R separated by h from a circular source of
4 radius ρ

Case #	R	h	ρ	Vega-Carrillo (1996)	Thabet, et. al. (2020)	Conway (2006)	General Method (n=360)
1	1	1	1	0.1161	0.1165	0.1161054	0.1161054
2	4	1	1	0.3761	0.3774	0.3761319	0.3761319
3	1	5	1	0.0094	0.0095	0.0094456	0.0094456
4	8	5	1	0.2342	0.2350	0.2341957	0.2341957
5	2.54	5	0.3	0.0541	0.0543	0.0541240	0.0541240
6	2.54	20	0.3	0.0040	0.0040	0.0039835	0.0039835
7	2.54	5	2	0.0501	0.0503	0.0501442	0.0501442
8	2.54	10	2	0.0150	0.0150	0.0149857	0.0149857
9	2.54	20	2	0.0039	0.0040	0.0039553	0.0039553

5

6 **7.4. Disk detector with respect to a parallel offset disk source**

7 The geometrical efficiency associated with a disk source whose axis is parallel to the axis of a disk detector was
8 computed according to Section 6 and compared to published results, Conway (2006) in Table 7. The circular disk
9 detector was modeled as a 360-sided polygon and the angular integration in eq. (40) and eq. (45) used 800 steps
10 with a two point gaussian integration scheme. Only ten digits to the right of the decimal point were retained in
11 Table 7, although in most cases agreement between the results extended to several more digits. Results from the
12 general method matched Conway's results, in all cases except case #8. When the number of sides of the polygon
13 was increased from 360 to 800 for case #8, results from the general method matched Conway's results to 11 digits
14 to the right of the decimal point, as shown in Case #8a. The agreement of the results in Table 7 shows that the
15 accuracy of the general method is only limited by the number of sides of the representative polygon and numerical
16 processing error.

17

18

19

20

21

22

23

24

25

26

27

1 Table 7. Geometrical efficiency of a disk detector of radius R separated by h from a parallel disk source of radius p
 2 offset by distance d

Case #	ρ	h	R	d	Conway (2006)	General Method (360-sided polygon)
1	1.0	1.0	0.5	0	0.0345720168	0.0345720168
2	1.0	1.0	0.5	0.2	0.0339484847	0.0339484847
3	1.0	1.0	0.5	0.4	0.0321294982	0.0321294982
4	1.0	1.0	0.5	0.6	0.0292784973	0.0292784973
5	1.0	1.0	0.5	0.8	0.0256782337	0.0256782337
6	1.0	1.0	0.5	1.0	0.0217032254	0.0217032254
7	1.0	1.0	2.0	0	0.2620768484	0.2620768484
8	1.0	1.0	2.0	0.5	0.2539076886	0.2539076885
8a	1.0	1.0	2.0	0.5	0.25390768855	0.25390768855 (800-sided polygon)
9	1.0	1.0	2.0	1.0	0.2284050042	0.2284050042
10	1.0	1.0	2.0	2.0	0.1357136065	0.1357136065
11	1.0	1.0	2.0	5.0	0.0094641787	0.0094641787
12	1.0	1.0	2.0	10.0	0.0010424862	0.0010424862
13	1.0	5.0	2.0	1.0	0.0334471117	0.0334471117
14	1.0	5.0	2.0	5.0	0.0143513580	0.0143513580
15	1.0	5.0	2.0	10.0	0.0036868176	0.0036868176
16	1.0	5.0	2.0	20.0	0.0005775649	0.0005775649

3

4 Conclusion

5 A general method to compute solid angle was developed that uses the attitude transformation of an axis that
 6 slews about a solid angle region. This method uses the results of Ishlinskii's theorem to establish the relationship
 7 between the solid angle and the region swept out by a slewing axis. Once the solid angle region is defined by a set
 8 of points on its perimeter, the Pivot Parameter method is used to compute the transformation of the slewing
 9 motion of the axis about the closed path. After the axis completes its closed path motion and returns to its initial
 10 orientation, the resulting rotation about the axis is the solid angle of the enclosed region. The method was applied
 11 to the solid angle of a disk detector with respect to a point source at an arbitrary location. Since the Pivot
 12 Parameter method involves great circle arc slews that connect the points that define the solid angle region, the
 13 circular disk was modeled as an n-sided polygon of area equal to that of the disk. The Pivot Parameter method
 14 yields the exact solid angle of the polygon, which is a very good approximation to the solid angle of the disk. A
 15 scale change applied to the polygon enables it to represent an elliptical shaped disk and permits the solid angle of
 16 the elliptical region to be evaluated exactly like the circular disk. A line source was modeled by a number of point
 17 sources distributed uniformly along the line. The average of the solid angles associated with the point sources
 18 provided the average solid angle of the line source. The average solid angle of a disk detector-source system
 19 having parallel axes was also obtained. Published test cases involving point, line and disk sources, were used to
 20 help establish the accuracy of this new method. If higher accuracy is required, the number of sides of the
 21 representative polygon can be increased such that the polygon represents the disk to a higher fidelity.
 22 Computation effort is not great, since it requires only a single 180-degree rotation per side of the polygon to
 23 obtain the associated attitude transformation of the axis. This new method is not limited to disk shaped sources,
 24 since any source geometry can be represented by a distribution of source points and any detector shape can be
 25 modeled as a set of perimeter points. Therefore, this method can treat any source-detector geometry desired.
 26 The method can be implemented using the two point gaussian integration algorithm or any suitable software
 27 integration package. A significant advantage of this new method is that it does not involve special mathematical

1 functions, integrals, or power series. This general solid angle computation method can be implemented easily in
2 computer simulations to compute solid angles that are needed in diverse disciplines, such as, radiant heat transfer,
3 particle scattering cross sections, electric and magnetic field strength, ligand size evaluation, rendering of 3-
4 dimensional objects in computer graphics, as well as calibrating the strength of radioisotopes. Since the proposed
5 general method can treat any geometric configuration, it can be applied to future solid angle calculation problems
6 that are not yet defined.

7

8 **References**

- 9 Abbas, M. I., "Analytical Calculations of the Solid Angle Subtended by a Circular Detector at Linear Sources,"
10 Scientific Publication of the State University of Novi Pazar Ser. A: Apl. Math Inform. And Mech. 10, 1, 17-23, (2018).
- 11 Conway, J. T., "Generalizations of Ruby's formula for the geometric efficiency of a parallel-disk source and detector
12 system," Nuclear Instruments and Methods Physics Research Section A: Accelerators, Spectrometers, Detectors,
13 and Associated Equipment 562, 146-153, (2006).
- 14 Conway, J. T., "Analytical solution for the solid angle subtended at any point by an ellipse via a point source
15 radiation vector potential," Nuclear Instruments and Methods in Physics Research A 614, 17-27 (2010a).
- 16 Conway, J. T., "Geometric efficiency for a circular detector and a linear source of arbitrary orientation and
17 position," Nuclear Instruments and Methods in Physics Research A 622, 555-566, (2010b).
- 18 Gardner, R. P., Carnesale, A., "The solid angle subtended at a point by a circular disk," Nuclear Instruments and
19 Methods 73, Issue 2, 228-230, (1969).
- 20 Gardner, R. P., and Verghese, K., "On the Solid Angle Subtended by a Circular Disc," Nuclear Instruments and
21 Methods 93, 163-167, (1971).
- 22 Ishlinkskii, A. Yu., "The Mechanics of Special Gyroscopic Systems," Izd. Akad. Nauk, UkrSSR, Kiev, (1952).
- 23 Patera, R. P., "Attitude propagation for a slewing angular rate vector," Journal of Guidance, Control and Dynamics
24 33, No. 6, 1847-1855, Nov.-Dec. (2010).
- 25 Patera, R. P., "New fundamental parameters for attitude representation," Advances in Space Research 60, 557-
26 570, (2017).
- 27 Patera, R. P., "Attitude kinematics using slewing transformation of a single axis," Advances in Space Research 66,
28 1460-1474, (2020).
- 29 Paxton, F., "Solid Angle Calculation for a Circular Disk," The Review of Scientific Instruments 30, No. 4, 254-258,
30 April (1959).
- 31 Ruby, L., and Rechen, J. B., "A simpler approach to the geometrical efficiency of a parallel-disk source and detector
32 system," Nuclear Instruments and Methods 58, Issue 2, 345-346, (1968).
- 33 Selim, Y. S. and Abbas, M. I., "Source-Detector Geometrical Efficiency," Radiat. Phys. Chem. 44, No. 1/2, 1-4,
34 (1994).
- 35 Thabet, A. A., Hamawy, A., and Badawi, M. S., "New Mathematical Approach to Calculate the Geometrical
36 Efficiency Using Different Radioactive Sources with Gamma-ray Cylindrical Shape Detectors," Nuclear Engineering
37 and Technology 52, Issue 6, 1271-1276, (2020).

1 Timus, D. M., Prata, M. J., Kalla, S. L., Abbas, M. I., Oner, F., and Galiano, E., "Some further analytical results on the
2 solid angle subtended at a point by a circular disk using elliptic integrals," Nuclear Instruments and Methods in
3 Physics Research A 580, 149-152 (2007).

4 Vega-Carrillo, H. R., "Geometrical efficiency for a parallel disk source and detector," Nuclear Instruments and
5 Methods Physics Research, Section A, Accelerator, Spectrometer. Detector, Associated Equipment 371, 535-537,
6 (1996).

7

8

9